Journal of Solid State Chemistry 183 (2010) 1258–1265

Contents lists available at ScienceDirect

Journal of Solid State Chemistry

journal homepage: www.elsevier.com/locate/jssc

# Synthesis and structural characterization of $A_3In_2Ge_4$ and $A_5In_3Ge_6$ ($A$=Ca, Sr, Eu, Yb)—New intermetallic compounds with complex structures, exhibiting Ge–Ge and In–In bonding

Tae-Soo You, Svilen Bobev *

*Department of Chemistry and Biochemistry, University of Delaware, Newark, DE 19716, USA*

ARTICLE INFO

*Article history:*
Received 17 February 2010
Received in revised form
19 March 2010
Accepted 27 March 2010
Available online 2 April 2010

*Keywords:*
Polar intermetallics
Crystal structure
Single-crystal X-ray diffraction
Electronic structure calculations

ABSTRACT

Reported are the synthesis and the structural characterization of four new polar intermetallic phases, which exist only with mixed alkaline-earth and rare-earth metal cations in narrow homogeneity ranges. $(Sr_{1-x}Ca_x)_5In_3Ge_6$ and $(Eu_{1-x}Yb_x)_5In_3Ge_6$ ($x \approx 0.7$) crystallize in the orthorhombic space group *Pnma* with two formula units per unit cell (own structure type, Pearson symbol *oP*56). The lattice parameters are as follows: $a$=13.109(3)–13.266(3) Å, $b$=4.4089(9)–4.4703(12) Å, and $c$=23.316(5)–23.557(6) Å. $(Sr_{1-x}Ca_x)_3In_2Ge_4$ and $(Sr_{1-x}Yb_x)_3In_2Ge_4$ ($x \approx 0.4$–0.5) adopt another novel monoclinic structure-type (space group *C*2/*m*, $Z$=4, Pearson symbol *mS*36) with lattice parameters in the range $a$=19.978(2)–20.202(2) Å, $b$=4.5287(5)–4.5664(5) Å, $c$=10.3295(12)–10.3447(10) Å, and $\beta$=98.214(2)–98.470(2)°, depending on the metal cations and their ratio. The polyanionic sub-structures in both cases are based on chains of $InGe_4$ corner-shared tetrahedra. The $A_5In_3Ge_6$ structure ($A$=Sr/Ca or Sr/Yb) also features $Ge_4$ tetramers, and isolated In atoms in nearly square-planar environment, while the $A_3In_2Ge_4$ structure ($A$=Sr/Ca or Eu/Yb) contains zig-zag chains of In and Ge strings with intricate topology of *cis*- and *trans*-bonds. The experimental results have been complemented by tight-binding linear muffin-tin orbital (LMTO) band structure calculations.



## 1. Introduction

The number of ternary intermetallic compounds in the systems *AE*–In–Ge and *RE*–In–Ge (*AE*=alkaline-earth; *RE*=rare-earth metals) is surprisingly small, given the vast available phase space and the many known binaries [1]. Surveying the structures of the structurally characterized compounds, one finds that the most ubiquitous one is the tetragonal $RE_2InGe_2$ ($Mo_2FeB_2$ type, Pearson symbol *tP*10) [2,3]. This structure is realized for almost all early to mid-late lanthanides. Other rare-earth metal rich compounds, such as the body-centered tetragonal $RE_3(In,Ge)_5$ ($In_5Bi_3$ type, Pearson symbol *tI*32) [4], $RE_3(In,Ge)_2$ ($Gd_3Ga_2$ type, Pearson symbol *tI*80) [4b,5], and $RE_{11}(In,Ge)_{10}$ ($Ho_{11}Ge_{10}$ type, Pearson symbol *tI*84) [4a,6], appear to form with La and Ce only. The nominally divalent Eu is reported to form EuInGe (own orthorhombic type, Pearson's symbol *oP*12), isostructural with SrInGe [7]. Two other relatively common structure types, that of the cubic clathrate-I (Pearson symbol *cP*54) and clathrate-IX (Pearson symbol *cP*132) are epitomized by $Ba_8(In,Ge)_{46}$ [8] and $Ba_6(In,Ge)_{25}$ [9], respectively. Guloy's pioneering work with mixed cations brought the first Ca-containing indium-germanides, seen on the examples of $SrCa_2In_2Ge$ [10] and $Ca_2LiInGe_2$ (Pearson symbol *oP*24) [11].

As part of our ongoing efforts in structure-property relationships in Zintl phases and intermetallics, we recently began exploring the quaternary *AE*–*RE*–In–Ge phase diagrams. We have already reported on several new phases, which were synthesized for the first time and structurally characterized: $(Eu_{1-x}Ca_x)_4In_3Ge_4$ ($0.3 \le x \le 0.7$), $(Eu_{1-x}Ca_x)_3In_2Ge_3$ ($0.7 \le x \le 0.9$), and $(Ca_{1-x}Yb_x)_8In_5Ge_8$ ($x \approx 0.4$) [12]. Notably, these new phases were found to exist in mixed-cation systems only. An analysis of their crystal structures showed that they are intergrowths of $Mo_2FeB_2$-like and TiNiSi-like fragments, and can be described as $A_{2[n+m]}In_{2n+m}Ge_{2[n+m]}$ ($A$=Ca, Sr, Eu, Yb), i.e., members of a homologous series. In this paper, we report the results from our efforts to synthesize higher order homologues and/or to employ different combinations of metal cations. As detailed in the next pages, these studies did not yield the sought-after compounds; instead the new phases $(Sr_{1-x}Ca_x)_5In_3Ge_6/(Eu_{1-x}Yb_x)_5In_3Ge_6$ ($x \approx 0.7$) and $(Sr_{1-x}Ca_x)_3In_2Ge_4/(Sr_{1-x}Yb_x)_3In_2Ge_4$ ($x \approx 0.4$–0.5) were obtained, dubbed short the "5-3-6" and "3-2-4" phases, respectively. Herein, we present the synthetic efforts and the single-crystal structures of these polar intermetallics and discuss the apparent cation sensitivity of these complex structures with mixtures of

* Corresponding author. Fax: +1 302 831 6335.
*E-mail address:* bobev@udel.edu (S. Bobev).

0022-4596/$ - see front matter © 2010 Elsevier Inc. All rights reserved.
doi:10.1016/j.jssc.2010.03.036

chemically similar, but spatially different cations. The experimental findings are confirmed by electronic structure calculations, which are indicative of chemical bonding with substantial cation contributions.

## 2. Experimental

### 2.1. Synthesis

Handling of the starting materials (pure Ca and Sr from Sigma-Aldrich, Eu, Yb and Ge from Alfa, used as-received) was carried out inside an argon-filled glove box or under vacuum. In a typical experiment, a mixture of the elements with the desired stoichiometric ratio (total weight ca. 500 mg) was loaded in a 2 $cm^3$ alumina crucible, which was then topped off with ca. 2 grams In (Alfa, shots). This ensures 10–15 fold excess of In (with respect to the alkaline- or rare-earth metal) as a flux. The crucible was subsequently enclosed and flame-sealed in an evacuated fused silica ampoule.

The title compounds were discovered in the attempts to substitute Eu or Ca with other rare-earth or alkaline-earth metals, following the optimized synthetic scheme, previously employed for growing crystals of $(Eu_{1-x}Ca_x)_4In_3Ge_4$ and $(Eu_{1-x}Ca_x)_3In_2Ge_3$ [12]. This procedure involved heating the mixture of elements to temperature 1223 K at a rate of 60°/h, allowed to homogenize for 10–12 h, and followed by a slow cooling to 773 K at rates of 3–10°/h. Then, the silica ampoules were taken out from a furnace and instantly centrifuged to remove the molten flux, allowing for the isolation of small needle-shaped crystals with silver luster. While across-the-board efforts were not made to explore the homogeneity ranges of these phases, our experiments suggest that $(Sr_{1-x}Ca_x)_5In_3Ge_6$/$(Eu_{1-x}Yb_x)_5In_3Ge_6$ form predominantly from Ca- or Yb-rich mixtures, i.e., where ratio of Sr (Eu) to Ca (Yb) ≈ 1:2. On the other hand, $(Sr_{1-x}Ca_x)_3In_2Ge_4$/$(Sr_{1-x}Yb_x)_3In_2Ge_4$ were obtained in higher yields from reactions with cation ratios ranging from Sr/Ca ≈ 1:1 to Sr/Ca ≈ 3:2, and Sr/Yb ≈ 5:3, respectively. The reactions aimed to synthesize pure ternary compounds with either structure or to employ other ratios failed. Based on the above, we can speculate that both the "5-3-6" and "3-2-4" phases exist in narrow homogeneity ranges.

All attempts to synthesize isotypic compounds with different metals were unsuccessful – they yielded known binary or ternary compounds – $Yb_2InGe_2$ [2,13], $EuGe_2$ [14], CaGe [15], $CaGe_2$ [16], $BaIn_4$ [17], being the most recurring ones.

### 2.2. X-ray crystallography

X-ray powder diffraction patterns were taken at room temperature on a Rigaku MiniFlex powder diffractometer using Cu $K\alpha$ radiation ($\theta-\theta$ scan mode with a step-size of 0.05° and rates of 5 s/step). The diffractograms were primarily used to assess the phase purity, an analysis that was carried out using the JADE 6.5 package. The observed peak-positions and the peaks' relative intensities matched well with those calculated from the single-crystal work. Since the powder diffractometer was enclosed and operated inside a nitrogen-filled glove box, we were also able to assess the air-(moisture) sensitivity of the new materials. According to powder patterns collected for specimens kept under inert atmosphere and after 72 h exposure to air, the title compounds are air-stable over this period of time.

Single-crystal X-ray diffraction data were collected at 200 K on a Bruker SMART CCD-based diffractometer. Several crystals from each batch were selected and checked for quality by rapid scans, before the best ones were chosen for further analysis. Monochromated Mo $K\alpha_1$ radiation ($\lambda$=0.71073 Å) was used, and data collections were handled in batch runs at different $\omega$ and $\phi$ angles, controlled by the *SMART* software [18]. Frame width was 0.3–0.4° in $\omega$ and $\theta$ with data acquisition rate of 8-12 sec/frame. The angular range in $2\theta$ was from ca. 5° to 60°. Intensities were extracted and corrected for Lorentz and polarization effects using the *SAINT* program [19]. Semi-empirical absorption correction based on equivalents was applied using *SADABS* [20]. The structure factors were sorted and merged by the program *XPREP* in the *SHELXTL* software package [21], which was also employed in the space group determination. The structures were solved by direct methods and refined to convergence by full matrix least-squares methods on $F^2$. Refined parameters included the scale factor, the atomic positions with anisotropic displacement parameters, and occupancy factors for the mixed cation positions. Standardization of the coordinates was done with the aid of *STRUCTURE TIDY* [22]. Relevant crystallographic data for six data collections are given in Tables 1 and 2. Final positional and equivalent isotropic displacement parameters, and selected interatomic distances for representative members of the "5-3-6" and "3-2-4" structures are listed in Tables 3 and 4, respectively. CIFs have also been deposited with Fachinformationszentrum Karlsruhe, 76344 Eggenstein-Leopoldshafen, Germany, (fax: (49)7247-808-666; e-mail: crysdata@fiz.karlsruhe.de) with depository numbers: CSD-421498 for $Sr_{1.50(1)}Ca_{3.50}In_3Ge_6$, CSD-421499

**Table 1**
Selected single-crystal data collection and structure refinement parameters for the "5-3-6" phases $(Sr_{1-x}Ca_x)_5In_3Ge_6$ ($x$=0.68, 0.70) and $(Eu_{1-x}Yb_x)_5In_3Ge_6$ ($x$=0.67).

| Empirical formula | $Sr_{1.50(1)}Ca_{3.50}In_3Ge_6$ | $Sr_{1.60(1)}Ca_{3.40}In_3Ge_6$ | $Eu_{1.65(1)}Yb_{3.35}In_3Ge_6$ |
|---|---|---|---|
| Formula weight, $Z$=4 | 1051.71 | 1056.46 | 1610.42 |
| Crystal system | | Orthorhombic | |
| Space group | | *Pnma*, no. 62 | |
| Temperature (K) | | 200 | |
| Unit cell dimensions (Å) | $a$=13.244(2) | $a$=13.266(4) | $a$=13.109(3) |
| | $b$=4.4603(6) | $b$=4.4703(12) | $b$=4.4089(9) |
| | $c$=23.505(3) | $c$=23.557(6) | $c$=23.316(5) |
| Volume (Å$^3$) | 1388.5(3) | 1397.0(6) | 1347.7(5) |
| Density (calculated, g/cm$^3$) | 5.03 | 5.02 | 7.94 |
| Absorption coefficient (cm$^{-1}$) | 237.7 | 248.2 | 486.7 |
| Data/restraints/parameters | 1943/0/90 | 1624/0/90 | 2269/0/89 |
| $R^*$ indices ($I>2\sigma_I$) | $R_1$=0.036 | $R_1$=0.047 | R1=0.037 |
| | $wR_2$=0.054 | $wR_2$=0.088 | $wR_2$=0.068 |
| $R^*$ indices (all data) | $R_1$=0.058 | $R_1$=0.086 | $R_1$=0.054 |
| | $wR_2$=0.060 | $wR_2$=0.102 | $wR_2$=0.074 |
| Goodness-of-fit on $F^2$ | 1.027 | 1.055 | 1.040 |
| Largest diff. peak/hole (e/Å$^3$) | 1.91/−1.60 | 2.43/−1.67 | 2.71/−4.05 |

*$R_1=\sum||F_o|-|F_c||/\sum|F_o|$; $wR_2=[\sum[w(F_o^2-F_c^2)^2]/\sum[w(F_o^2)^2]]^{1/2}$, where $w=1/[\sigma^2F_o^2+(A-P)^2+B-P]$, and $P=(F_o^2+2F_c^2)/3$; A and B – weight coefficients.

**Table 2**
Selected single-crystal data collection and structure refinement parameters for the "3-2-4" phases $(Sr_{1-x}Ca_x)_3In_2Ge_4$ ($x=0.39$, 0.49) and $(Eu_{1-x}Yb_x)_3In_2Ge_4$ ($x=0.37$).

| Empirical formula | $Sr_{1.53(1)}Ca_{1.47}In_2Ge_4$ | $Sr_{1.83(1)}Ca_{1.17}In_2Ge_4$ | $Sr_{1.89(1)}Yb_{1.11}In_2Ge_4$ |
|---|---|---|---|
| Formula weight, $Z=4$ | 712.98 | 727.24 | 877.68 |
| Crystal system | | Monoclinic | |
| Space group | | *C*2/*m*, no. 12 | |
| Temperature (K) | | 200 | |
| Unit cell dimensions (Å) | $a=19.9778(17)$ | $a=20.202(2)$ | $a=19.980(2)$ |
| | $b=4.5522(4)$ | $b=4.5664(5)$ | $b=4.5287(5)$ |
| | $c=10.3323(9)$ | $c=10.3447(10)$ | $c=10.3295(12)$ |
| | $\beta=98.444(2)^\circ$ | $\beta=98.470(2)^\circ$ | $\beta=98.214(2)^\circ$ |
| Volume (Å$^3$) | 929.46(14) | 935.40(17) | 925.04(19) |
| Density (calculated, g/cm$^3$) | 5.09 | 5.16 | 6.30 |
| Absorption coefficient (cm$^{-1}$) | 270.6 | 284.1 | 395.1 |
| Data/restraints/parameters | 1512/0/58 | 1498/0/58 | 1513/0/59 |
| $R^*$ indices ($I>2\sigma_I$) | $R1=0.046$ | $R1=0.051$ | $R1=0.041$ |
| | $wR_2=0.098$ | $wR_2=0.101$ | $wR_2=0.085$ |
| $R^*$ indices (all data)] | $R1=0.074$ | $R1=0.086$ | $R1=0.061$ |
| | $wR_2=0.110$ | $wR_2=0.114$ | $wR_2=0.093$ |
| Goodness-of-fit on $F^2$ | 1.058 | 1.064 | 1.054 |
| Largest diff. peak/hole (e/Å$^3$) | 4.47/−1.69 | 3.84/−1.87 | 2.76/−2.94 |

$^*$ $R1=\sum||F_o|-|F_c||/\sum|F_o|$; $wR_2=[\sum[w(F_o^2-F_c^2)^2]/\sum[w(F_o^2)^2]]^{1/2}$, where $w=1/[\sigma^2F_o^2+(A-P)^2+B-P]$, and $P=(F_o^2+2F_c^2)/3$; A and B – weight coefficients.

for $Sr_{1.60(1)}Ca_{3.40}In_3Ge_6$, CSD-421500 for $Eu_{1.65(1)}Yb_{3.35}In_3Ge_6$, CSD-421501 for $Sr_{1.53(1)}Ca_{1.47}In_2Ge_4$, CSD-421502 for $Sr_{1.83(1)}Ca_{1.17}In_2Ge_4$, CSD-421503 for $Sr_{1.89(1)}Yb_{1.11}In_2Ge_4$.

### 2.3. Electronic structure calculations

Tight-binding, linear muffin-tin orbital (TB-LMTO) calculations [23] were carried out using the LMTO47 program [24]. This package employs the atomic sphere approximation (ASA) method, in which space is filled with overlapping Wigner–Seitz (WS) atomic spheres [25]. The symmetry of the potential is considered spherical inside each WS sphere, and a combined correction is used to take into account the overlapping part [26]. The radii of WS spheres were obtained by requiring that the overlapping potential be the best possible approximation to the full potential, and were determined by an automatic procedure [26]. This overlap should not be too large because the error in kinetic energy introduced by the combined correction is proportional to the fourth power of the relative sphere overlap. The WS radii are as follows: for the "5-3-6" structure, Sr and Ca=2.13–2.17 Å, In=1.60–1.74 Å, Ge=1.50–1.64 Å; the "3-2-4" structure, Sr and Ca=2.09–2.22 Å, In=1.59–1.68 Å, Ge=1.50–1.56 Å; and for the hypothetical model of the "3-2-4" structure, Sr and Ca=1.84–2.23 Å, In=1.60–1.65 Å, Ge=1.47–1.55 Å. Exchange and correlation were treated by the local density approximation (LDA) [27]. All relativistic effects, except spin-orbit coupling, were taken into account by using a scalar relativistic approximation.

The density of states (DOS) plots are presented herein with the Fermi level set as a reference point at 0 eV. In order to evaluate various orbital interactions, the crystal orbital Hamilton populations (COHP) [28] were also calculated. The *k*-space integrations were conducted by the tetrahedron method [29], and the self-consistent charge density was obtained using 120–178 irreducible *k*-points in the Brillouin zone.

## 3. Results and discussion

### 3.1. "5-3-6" phase

The new compounds $(Sr_{1-x}Ca_x)_5In_3Ge_6$ and $(Eu_{1-x}Yb_x)_5In_3Ge_6$ ($x\approx0.7$) crystallize with the orthorhombic space group *Pnma*, adopting a new structure type (Pearson code *oP*56). This structure includes 14 crystallographically unique atomic positions in the asymmetric unit (Table 3). The crystal structure can be best viewed as a 3-dimensional anionic framework of In and Ge, and alkaline-earth or rare-earth cations occupying the space within it (Fig. 1 (a)).

The anionic framework consists of two different types of $[InGe_4]$ fragments: (1) In-centered tetrahedra of Ge (Fig. 1 (b)); and (2) In-centered squares of Ge atoms (Fig. 1 (c)). The $[InGe_4]$ tetrahedra are corner-shared in such a manner, that double $[In_2Ge_5]$ chains are formed. They propagate parallel to the crystallographic *b*-axis and are further linked to each other in the *ac*-plane via tetrameric "spacers", $Ge_4$. The latter have the topology of *cis*-butadiene, as shown in Fig. 1 (d). The In–Ge distances in the tetrahedral environments range from 2.672(2) to 2.877(3) Å, and are comparable to the sum of the corresponding covalent radii ($r_{In}=1.55$ Å; $r_{Ge}=1.22$ Å) [30]. However, longer In–Ge distances, thereby weaker In–Ge bonding interactions are observed in the square-planar $[InGe_4]$ fragment (Table 4). The Ge–Ge contacts ($d_{Ge-Ge}=2.528(2)$–$2.550(3)$ Å) match very well with those reported for single-bonded germanium, such as in $CaGe_2$ [16], SrInGe [7], $EuGe_2$ [14], $Ca_5Ge_3$ [31], $SrGe_2$ [32], $Ca_2LiInGe_2$ and $Sr_2LiInGe_2$ [11]. All In–Ge and Ge–Ge bond distances in $(Sr_{1-x}Ca_x)_5In_3Ge_6$ increase slightly as the composition becomes Sr-richer. These observations are in a good agreement with the earlier reports on the $(Eu_{1-x}Ca_x)_4In_3Ge_4$ and $(Eu_{1-x}Ca_x)_3In_2Ge_3$ series [12], where similar structural motifs are present as well. Just like them, the $A_5In_3Ge_6$ phase is stabilized by mixtures of two types of cations – Sr and Ca or Eu and Yb – which are chemically similar, but spatially different species. We note here that even without experimental evidence, the possibility for a varied valence state of the rare-earth metals can be easily ruled out: (1) the same structures can exist only with Sr and Ca, which cannot be in any other oxidation state; (2) $Eu^{2+}$ and $Yb^{2+}$ are the most commonly observed states for these ions in the weakly reducing atomic environment of polar intermetallic phases.

Five different cation sites are observed in the "5-3-6" phase (Fig. 2). They are never occupied by a single atom and are all refined as statistical mixtures. Table 3 lists the corresponding site occupation factors. *A*1, *A*4 and *A*5 positions appear to be preferred by the smaller $Ca^{2+}$ ($r=1.02$ Å) and $Yb^{2+}$ ($r=1.00$ Å) [33], while the *A*2 and *A*3 sites are preferentially occupied by the larger $Sr^{2+}$ ($r=1.17$ Å) and $Eu^{2+}$ ($r=1.16$ Å) [33], respectively. The *A*1 and *A*4

sites are surrounded by total of 10 Ge and In atoms, making the polyhedron appear somewhat as a ferrocene-like pentagonal prism. However, a small difference between the two must be pointed out—the *A*4 site is surrounded by 8 Ge and 2 In atoms, whereas the *A*1 site is surrounded by 6 Ge and 4 In atoms. The *A*2, *A*3 and *A*5 sites have a similar coordination mode of the central cation, which consists of five nearest or second-nearest Ge atoms forming a distorted square-pyramid. Moreover, the edges and/or faces of these pyramids are capped by In or Ge in the following way: in the case of the *A*5 site, five edges are capped by In, resulting in a total coordination number of 10; in the case of *A*2 and *A*3, seven additional atoms in close proximity of the pyramid bring the total coordination number to 12. Considering that, one can easily rationalize the cation distribution following the Pauling's rule, i.e., larger cations for the sites with coordination number of 12 (*A*2 and *A*3) and smaller cations for the sites with coordination number of 10 (*A*1, *A*4 and *A*5).

### 3.2. "3-2-4" phase

As mentioned already, the "5-3-6" phase was obtained only from mixtures rich in the smaller cations, e.g., Sr/Ca=1:2. When the ratio between the cations was equimolar or when the larger cations were in excess, the "3-2-4" phase was synthesized following the very same reaction conditions (notice how close compositionally they are). Up until now, we have structurally characterized $(Sr_{1-x}Ca_x)_3In_2Ge_4$ and $(Sr_{1-x}Yb_x)_3In_2Ge_4$ ($x \approx 0.4$–$0.5$), although $(Eu_{1-x}Yb_x)_3In_2Ge_4$ might exist as well.

The "3-2-4" phases crystallize in the monoclinic space group *C*2/*m* with a new structure type (Pearson code *mS*36). This structure is also complex, containing 9 crystallographically unique atom sites in the asymmetric unit, all in special positions

**Table 3**
Atomic coordinates and equivalent isotropic displacement parameters ($U_{eq}$)[a] from single-crystal structure refinements for $(Sr_{1-x}Ca_x)_5In_3Ge_6$ ($x=0.70$) and $(Sr_{1-x}Ca_x)_3In_2Ge_4$ ($x=0.49$).

| Atom | Wyckoff site | *x* | *y* | *z* | $U_{eq}$ (Å$^2$) | Sr/Ca ratio |
|---|---|---|---|---|---|---|
| $Sr_{1.50(1)}Ca_{3.50}In_3Ge_6$ | | | | | | |
| *A*1[b] | 4*c* | 0.0052(1) | 1/4 | 0.2142(1) | 0.011(1) | 0.126(8)/0.874 |
| *A*2[b] | 4*c* | 0.1255(1) | 1/4 | 0.0418(1) | 0.012(1) | 0.774(8)/0.226 |
| *A*3[b] | 4*c* | 0.2109(1) | 1/4 | 0.3419(1) | 0.011(1) | 0.519(8)/0.481 |
| *A*4[b] | 4*c* | 0.2820(1) | 1/4 | 0.1860(1) | 0.010(1) | 0.028(8)/0.972 |
| *A*5[b] | 4*c* | 0.4468(1) | 1/4 | 0.0592(1) | 0.010(1) | 0.055(8)/0.945 |
| In1 | 4*c* | 0.0152(1) | 1/4 | 0.6699(1) | 0.018(1) | |
| In2 | 4*c* | 0.1972(1) | 1/4 | 0.4791(1) | 0.011(1) | |
| In3 | 4*c* | 0.5854(1) | 1/4 | 0.6169(1) | 0.012(1) | |
| Ge1 | 4*c* | 0.1523(1) | 1/4 | 0.7693(1) | 0.011(1) | |
| Ge2 | 4*c* | 0.2024(1) | 1/4 | 0.5961(1) | 0.010(1) | |
| Ge3 | 4*c* | 0.3418(1) | 1/4 | 0.7512(1) | 0.012(1) | |
| Ge4 | 4*c* | 0.3741(1) | 1/4 | 0.6451(1) | 0.012(1) | |
| Ge5 | 4*c* | 0.3916(1) | 1/4 | 0.4438(1) | 0.011(1) | |
| Ge6 | 4*c* | 0.3936(1) | 1/4 | 0.9306(1) | 0.012(1) | |
| $Sr_{1.53(1)}Ca_{1.47}In_2Ge_4$ | | | | | | |
| *A*1[b] | 4*i* | 0.0085(1) | 0 | 0.3304(2) | 0.014(1) | 0.058(8)/0.942 |
| *A*2[b] | 4*i* | 0.1007(1) | 0 | 0.0102(1) | 0.013(1) | 0.648(8)/0.352 |
| *A*3[b] | 4*i* | 0.1833(1) | 0 | 0.6093(1) | 0.015(1) | 0.826(8)/0.174 |
| In1 | 4*i* | 0.2697(1) | 0 | 0.0840(1) | 0.016(1) | |
| In2 | 4*i* | 0.6313(1) | 0 | 0.2998(1) | 0.012(1) | |
| Ge1 | 4*i* | 0.2051(1) | 0 | 0.3015(1) | 0.012(1) | |
| Ge2 | 4*i* | 0.3981(1) | 0 | 0.2231(1) | 0.035(1) | |
| Ge3 | 4*i* | 0.4352(1) | 0 | 0.4774(1) | 0.012(1) | |
| Ge4 | 4*i* | 0.5097(1) | 0 | 0.1242(1) | 0.015(1) | |

[a] $U_{eq}$ is defined as one third of the trace of the orthogonalized $U_{ij}$ tensor.
[b] Refined as a statistical mixture of Sr and Ca.

**Table 4**
Selected bond distances (in Å) for $(Sr_{1-x}Ca_x)_5In_3Ge_6$ ($x=0.70$) and $(Sr_{1-x}Ca_x)_3In_2Ge_4$ ($x=0.49$).

| $Sr_{1.50(1)}Ca_{3.50}In_3Ge_6$ | | $Sr_{1.53(1)}Ca_{1.47}In_2Ge_4$ | |
|---|---|---|---|
| Atomic pair | Distance | Atomic pair | Distance |
| In2–Ge5 (1 × ) | 2.703(2) | In2–Ge1 (2 × ) | 2.716(1) |
| In2–Ge2 (1 × ) | 2.750(2) | In2–Ge4 (1 × ) | 2.815(3) |
| In2–Ge6 (2 × ) | 2.784(2) | In2–Ge3 (1 × ) | 2.822(3) |
| In3–Ge5 (2 × ) | 2.672(2) | In1–Ge2 (1 × ) | 2.755(3) |
| In3–Ge1 (1 × ) | 2.821(3) | In1–Ge1 (1 × ) | 2.757(3) |
| In3–Ge4 (1 × ) | 2.877(3) | In1–In1 (2 × ) | 2.910(3) |
| Ge2–Ge4 (1 × ) | 2.528(2) | Ge4–Ge4 (1 × ) | 2.538(2) |
| Ge1–Ge3 (1 × ) | 2.545(3) | Ge3–Ge3 (1 × ) | 2.561(2) |
| Ge3–Ge4 (1 × ) | 2.550(3) | Ge2–Ge4 (1 × ) | 2.594(2) |
| | | Ge2–Ge3 (1 × ) | 2.622(2) |
| In1–Ge4 (1 × ) | 2.864(3) | | |
| In1–Ge3 (1 × ) | 2.953(3) | | |
| In1–Ge1 (1 × ) | 2.763(3) | | |
| In1–Ge2 (1 × ) | 3.034(3) | | |

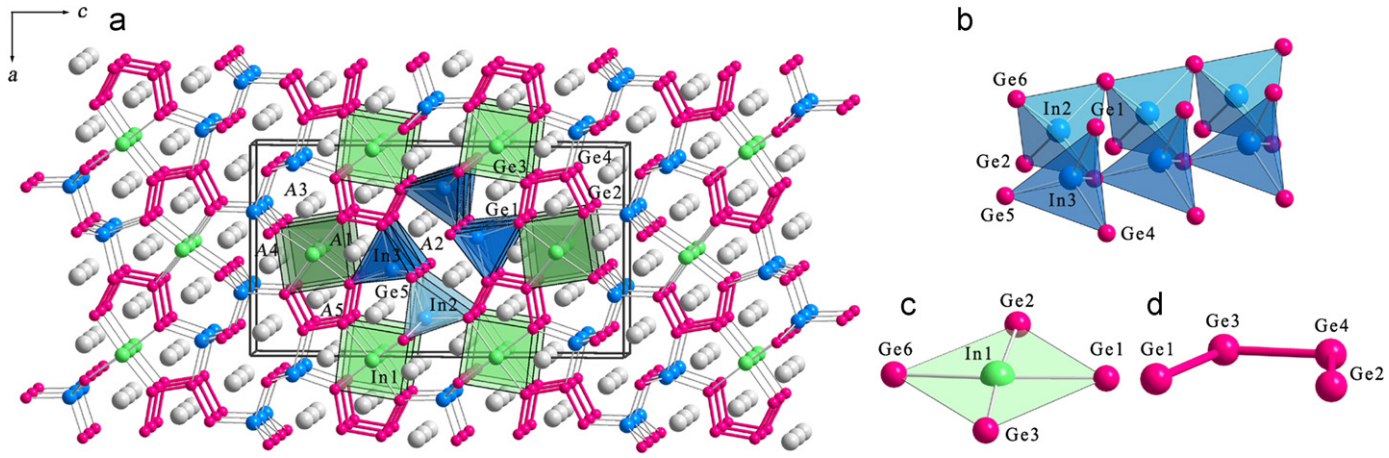


**Fig. 1.** (a) Combined ball-and-stick and polyhedral representations of the crystal structure of the orthorhombic $(Sr_{1-x}Ca_x)_5In_3Ge_6$ ("5-3-6" phase), viewed down the *b*-axis. Unit cell is outlined. The anionic substructure is made up of the following fragments: corner-shared tetrahedral [$InGe_4$] chains, surrounding square-planar [$InGe_4$] and $Ge_4$ tetramers isosteric with 1,3-*cis*-butadiene. (b) Close up view, emphasizing the connectivity of [$InGe_4$] tetrahedra in the double-chains. (c) and (d) Magnified views of the distorted square-planar [$InGe_4$] fragment and the $Ge_4$ tetramers, respectively. Online color: tetrahedral In2/3 – blue; planar In1 – green; Ge – magenta; and cations – gray. (For interpretation of the references to color in this figure legend, the reader is referred to the web version of this article.)

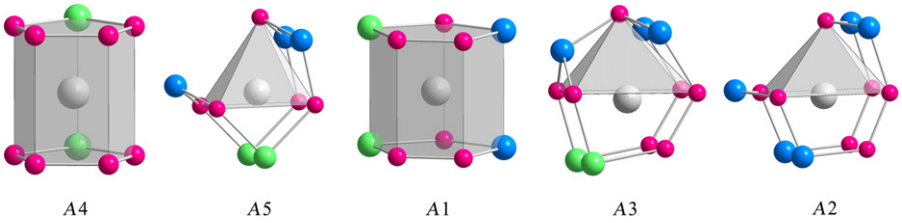


**Fig. 2.** Coordination polyhedra of the five cations in the "5-3-6" phase. The polyhedra are displayed in the descending order by volume. Online color: tetrahedral In2/3 – blue; planar In1 – green; Ge – magenta; and cations – gray. (For interpretation of the references to color in this figure legend, the reader is referred to the web version of this article.)

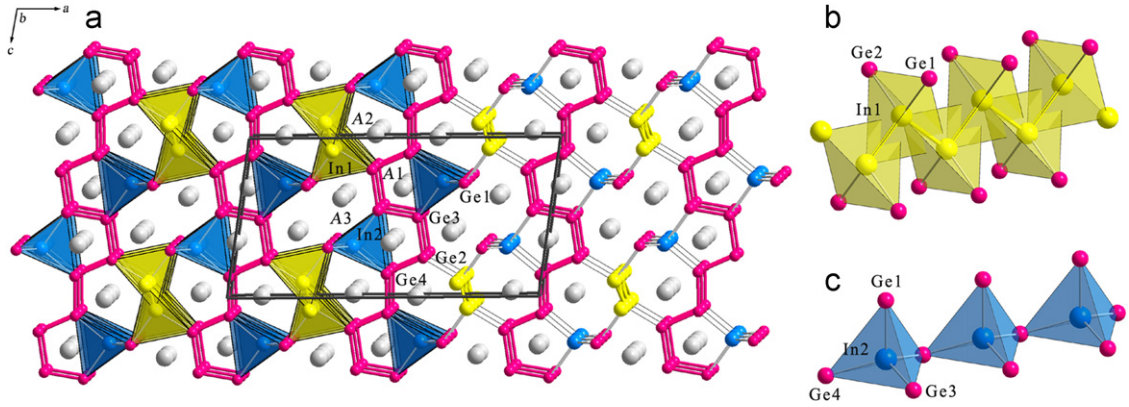


**Fig. 3.** (a) Combined ball-and-stick and polyhedral representations of the crystal structure of the orthorhombic $(Sr_{1-x}Ca_x)_3In_2Ge_4$ ("3-2-4" phase), viewed down the *b*-axis. Unit cell is outlined. The anionic substructure is made up of the following fragments: corner-shared tetrahedral $[InGe_4]$ chains, In zig-zag chains, and infinite Ge strings with *cis*- and *trans*-bonds in a complex $(tttctc)_n$ pattern. (b) and (c) Close up views, emphasizing the connectivity of $[InGe_4]$ tetrahedra and the interpenetrating tetrahedral $[In_2Ge_4]$ chains, respectively. Online color: In2 – blue; In1 – yellow; Ge – magenta; and cations – gray. (For interpretation of the references to color in this figure legend, the reader is referred to the web version of this article.)

(Table 3). The atomic arrangement is best explained as a 3-D polyanionic framework with cations located within the open channels (Fig. 3). Just like the "5-3-6" structure, there are $^1_\infty[InGe_3]$ chains of corner shared $InGe_4$-tetrahedra, which extend along the *b*-axis. These chains are joined together in a direction of the *c*-axis by infinite $^1_\infty[Ge_6]$ strings with multifaceted topology. One can designate the basic repeating unit here as $(tttctc)_n$, where *t* refers to the *trans*-, and *c* refers to the *cis*-conformation, respectively. Nearly identical Ge fragments are observed in the Li-containing compounds α-$Ca_2LiGe_3$, α-$Sr_2LiGe_3$ and $Eu_2LiGe_3$ [34], in which the special characteristics of the $^1_\infty[Ge_6]Li$ metal – its high ionic potential in particular – have been attributed as a key factor to the formation of such unique bonding pattern.

However, unlike those Li-containing compounds, in the "3-2-4" structure, the germanium $(tttctc)_n$ chains are not isolated, but connected to two other building blocks: (1) the above-mentioned chains of corner shared $InGe_4$-tetrahedra; and (2) infinite zig-zag chains of In atoms (In1) (Fig. 3(b)). This is a subtle, but important difference between the chains in α-$Ca_2LiGe_3$, where each Ge atom is two-bonded [34], and the $^1_\infty[Ge_6]$ chains here, where each Ge atom is three-bonded. A more careful analysis of the connectivity and the interatomic distances in these chains is the focus of the discussion in the next paragraph.

The In–Ge distances in $(Sr_{1-x}Ca_x)_3In_2Ge_4$, are "normal" and compare very well with those seen already for $(Sr_{1-x}Ca_x)_5In_3Ge_6$ (Table 4). The In–In bonds at ca. 2.90 Å match very well with those reported for other structures with zig-zag chains of In, such as $K_3Au_5In$ [35] and $KNa_3In_9$ [36]. However, the Ge–Ge distances, ranging from 2.538(2) to 2.622(2) Å, are slightly longer than those observed in the α-$Ca_2LiGe_3$, α-$Sr_2LiGe_3$ and $Eu_2LiGe_3$ ($d_{Ge-Ge}$=2.528(2)–2.550(3) Å) [34], where π-delocalization of

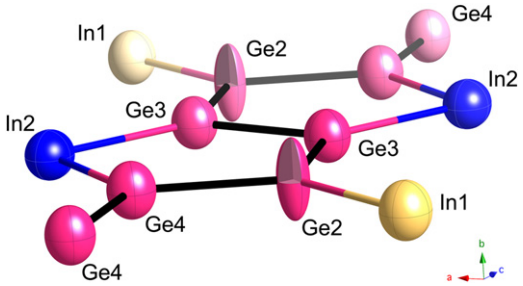


**Fig. 4.** A fragment of the anionic substructure of $(Sr_{1-x}Ca_x)_3In_2Ge_4$ ("3-2-4" phase), drawn with thermal ellipsoids (95% probability level). The abnormal elongation of the anisotropic displacement parameter of Ge2, which hints at the possibility for an offset from the mirror plane is clearly seen. For example, in the case of $Sr_{1.53(1)}Ca_{1.47}In_2Ge_4$, $U_{11}$=0.012(1), $U_{22}$=0.081(1), and $U_{33}$=0.012(1), respectively. Cations are omitted for clarity.

the Ge 4*p*-orbitals perpendicular to the plane of the chain must be considered. Given the extended distances and given the fact that Ge in a trigonal planar environment (parallel to the *ac* plane) is not an energetically favorable configuration, one might suspect that there is something unordinary about the refined structure. Indeed, a closer look at the anisotropic displacement parameters (ADP) of all In and Ge atoms (Fig. 4) provides some clues—all In and Ge exhibit well-behaved thermal ellipsoids, but Ge2. In the case of Ge2, its ADP is significantly elongated in direction perpendicular to the mirror plane, i.e., the *b*-axis. $U_{22}/U_{11} \approx 7$ is suggestive of a positional disorder, most likely a violation of the mirror symmetry, which could result in a small "buckling" of the chain at this point [37]. Such pyramidalization of 3-bonded germanium is not unprecedented [7], and is expected to diminish the energetically unfavorable effect of $\pi^*$-conjugation along the

chain. The possible driving force for a disorder at the Ge2 site is further discussed in the electronic structure section.

There are three crystallographically unique cation sites in the "3-2-4" structure, and their coordination polyhedra resemble those already mentioned for the "5-3-6" structure (Fig. 5). The cation at the *A*1 site is surrounded by 8 Ge and 2 In atoms in a pentagonal prismatic environment, nearly the same as the *A*1 and *A*4 sites in the "5-3-6" phase. The cation in the *A*3 site is 12-coordinated, similar to the *A*2 and *A*3 sites in the "5-3-6" phase. The *A*2 site also has a coordination number of 12; however, in this case the square-pyramid is formed by 3 Ge and 2 In atoms. Following the same geometric reasoning discussed previously for the "coloring" of the cation sites in the "5-3-6" structure, it is easy to predict that the sites with higher coordination numbers in the "3-2-4" structure (*A*2 and *A*3) will be preferred by the larger $Sr^{2+}$ cations, whereas the sites with fewer neighbors will be preferred by the smaller $Ca^{2+}$ or $Yb^{2+}$ cations. Indeed, as seen from Table 3, the 10-coordinated *A*1 refines as nearly fully occupied Ca, while the 12-coordinated *A*2 and *A*3 sites show preferential occupation by Sr. Based on the above observations, we can also rationalize the fact that the "3-2-4" phase forms with mixtures of cations dominated by the larger species, while the "5-3-6" phase is obtained from composition richer in the smaller cation—the former structure has 2 out of 3 *A*-sites with CN 12, vs. 2 out of 5 in the latter structure. Similar ideas, for instance, have also been established for the clathrates of types I-, and II-, where the proper selection of spatially different alkali-metal cations can be used for their rational synthesis [38].

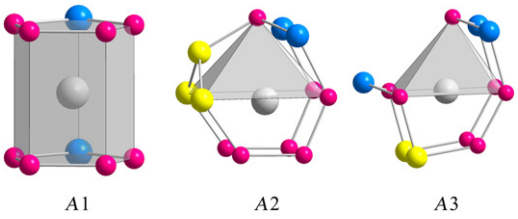


**Fig. 5.** Coordination polyhedra of the three cations in the "3-2-4" phase. The polyhedra are displayed in the descending order by volume. Online color: tetrahedral In2/3 – blue; planar In1 – green; Ge – magenta; and cations – gray. (For interpretation of the references to color in this figure legend, the reader is referred to the web version of this article.)

### 3.3. Bonding and electronic structure

To understand the chemical bonding and the electronic structures of the two novel structures, band-structure calculations were conducted using the TB-LMTO-ASA method [23]. For the "5-3-6" phase, calculations were performed using a structure model with an idealized composition "$Sr_3Ca_7In_6Ge_{12}$". For this purpose, the symmetry was lowered to $P2_1/m$, which allowed ordering of the cations, where Sr atoms occupy the *A*2 and a half of the *A*3 sites; Ca atoms cover the remaining cation positions. Lattice parameters and atomic coordinates were taken from $Sr_{1.50(1)}Ca_{3.50}In_3Ge_6$, since it has an identical composition as the structure model. DOS and COHP curves are plotted in Fig. 6 (a).

As seen from the plot of the total density of states (TDOS), there is no band gap at the Fermi level. There is, however, a local minimum (so called "pseudogap"), which is one of the typical characters of polar intermetallic phases [39]. Throughout the whole energy window, a strong valence orbital mixing is observed. In particular, significant contributions from Sr 5*s* and Ca 4*s* orbitals to the occupied states between −4 and 0 eV are noticeable. This behavior can be readily understood by recalling that in polar intermetallics and in many Zintl phases (extreme cases of "polarization") [40], the notion that the electropositive metals contribute *all* of their valence electrons to the anionic network formed by electronegative atoms may not be true [31,41]. This proves that the cations are not just space fillers in an atomic structure, but are intimately involved in chemical bonding, which is another distinct characteristic of the polar intermetallic phase [39].

The COHP curves (Fig. 6(a), middle) display the In2–Ge and In3–Ge bonding, i.e., atomic interactions within the two tetrahedral [$InGe_4$] units. These are differentiated from the In1–Ge interactions within the distorted square-planar [$InGe_4$] fragment. The COHP curves from two tetrahedra show very similar patterns and are nearly optimized at the Fermi level. On the other hand, the COHP curve from the distorted square-planar geometry represents an overall weaker interaction due to extended bond distances. The COHP curves displayed Fig. 6(a), right show two interatomic interactions between Ge atoms on the same anionic plane and between Ge and surrounding cations forming a trigonal prismatic environment. As can be seen, the Ge–Ge COHP curve shows an antibonding character at the Fermi level. This type of antibonding character was also observed from $Ge_2$-dimers in the

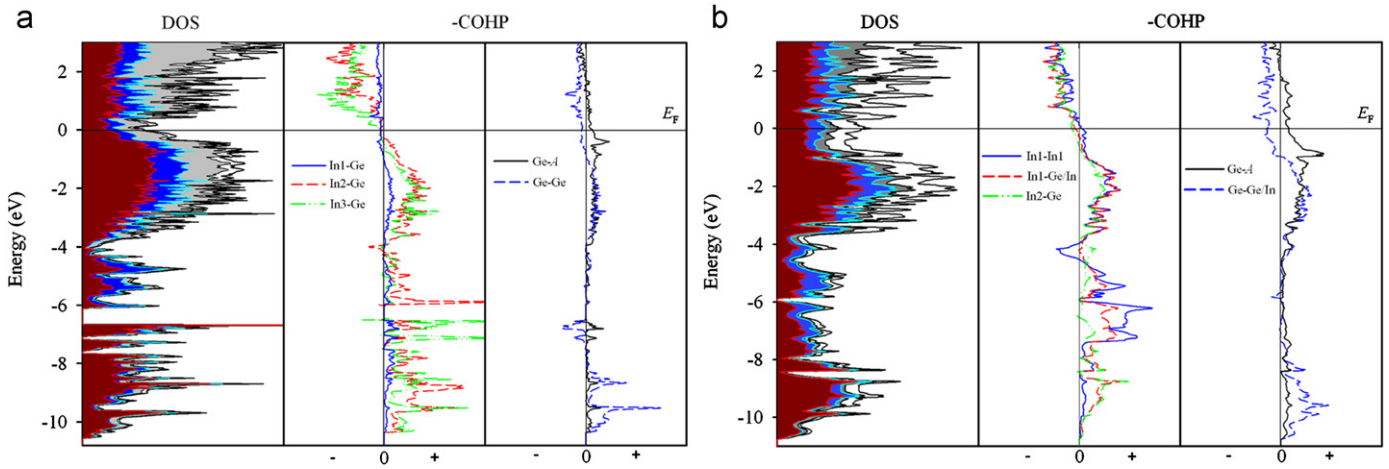


**Fig. 6.** DOS and COHP curves for the "5-3-6" phase (a), and for the "3-2-4" phase (b). Total DOS curves are shown with a solid line; partial DOS are shown as shaded areas. $E_F$ (solid line) is the energy reference at 0 eV. In the COHP curves, the values are inverted so that the "+" regions represent bonding interactions, and the "–" regions represent antibonding interactions, respectively. Color online: partial DOS of Sr, Ca, In and Ge are represented by the areas shaded in white, gray, blue, and red, respectively. (For interpretation of the references to colour in this figure legend, the reader is referred to the web version of this article.)

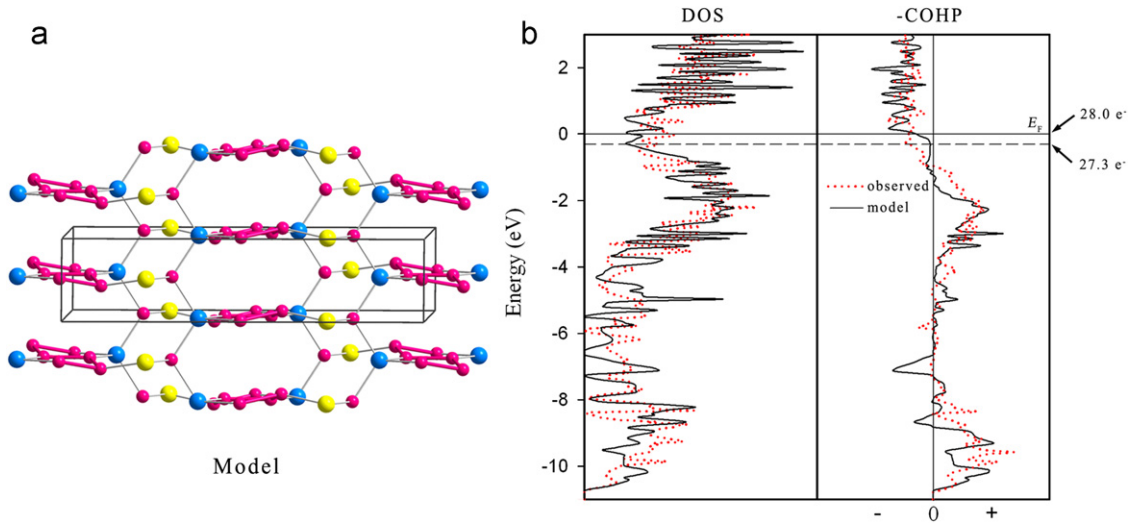


**Fig. 7.** (a) A model "3-2-4" structure, taking into consideration the possibility for "puckering" of the 3-bonded planar fragment. Cations are not shown for clarity. Color online: In1 – yellow; In2 – blue; and Ge – magenta. (b) Side-by-side comparison of the total DOS and the Ge–Ge/In COHP curves of the actual structure (dotted line) and the model structure (solid line). $E_F$ is the energy reference at 0 eV. In the COHP curves, the values are inverted so that the "+" regions represent bonding interactions, and the "–" regions represent antibonding interactions, respectively. (For interpretation of the references to color in this figure legend, the reader is referred to the web version of this article.)

$(Eu_{1-x}Ca_x)_4In_3Ge_4$ and $(Eu_{1-x}Ca_x)_3In_2Ge_3$ phases [12]. As discussed therein, this antibonding character is caused by the 3-bonded Ge atom in a trigonal planar local environment, instead of being in a preferred pyramidal, as observed in the corrugated $[Ge_2]^{2-}$ layers in $EuGe_2$ and $CaGe_2$ [14,16]. However, this antibonding character is compensated by the bonding character between Ge and cations in a trigonal prismatic environment, which retains its bonding character up to ca. 1.5 eV.

For the "3-2-4" phase, we used two structure models for calculations in order to address the open questions regarding the ADP and possible positional disorder at the Ge2 site. First, we used the observed *C*2/*m* structure, with the coordinates from the actual refinements given in Table 2. In this treatment, the $(tttctc)_n$ chains of Ge are constrained within the *ac* plane, as shown in Fig. 3 and as discussed earlier. We also did calculations for a model, presented schematically in Fig. 7(a), of a hypothetical structure with a pyramidal local environment at the Ge2 site. In this arrangement, the Ge2 atoms were offset by ca. 0.4 Å from $y=0$ along the *b*-axis, leading to a small *in-phase* corrugation between eclipsed Ge chains. Such calculations were carried out in the space group $P2_1/c$, instead of $P2_1/a$, which is the *klassengleiche* subgroup IIa for *C*2/*m*. The reason for interchanging the *a* and *c* axes here is a deficiency in the LMTO47 code, which allows only space groups in their standard settings. For both models, Ca atoms were assigned only to the *A*1 site, whereas Sr atoms are assigned to the *A*2 and *A*3 sites, resulting in an idealized composition of "$Sr_2CaIn_2Ge_4$". Lattice parameters and atomic positions were taken from $Sr_{1.83(1)}Ca_{1.17}In_2Ge_4$ (Table 2).

DOS and COHP curves from the calculations for the structure with atomic position from the single-crystal refined data are illustrated in Fig. 6(b). The overall appearance of DOS curves are similar to those of the "5-3-6" structure, including a local DOS minimum at around Fermi level and a strong cation *s* orbital involvement to the occupied orbital state between −3.5 and 0 eV. Two noticeable differences are the significantly increased TDOS at the Fermi level, and the *s* orbital interactions mostly between anions observed at ca. −6 eV.

The atomic interactions within an anionic framework and between cations and anions are studied by COHP analysis as well. The COHP curves of the In1–In1 zig-zag chain and In1–Ge/In within "bow-tie" like tetrahedra are nearly optimized at the Fermi level, whereas a COHP curve of In2–Ge from the other $[InGe_4]$ tetrahedra attached to the Ge chain shows a weak antibonding character (Fig. 6(b), middle). Two averaged COHP curves between Ge and Ge/In and between Ge and cations are plotted in Fig. 6(b), right. Ge–In/Ge COHP shows a strong antibonding character, which is partially compensated by the strong bonding between the Ge and the cations. Nonetheless, the large TDOS and the strong antibonding character of Ge-anion COHP at the Fermi level is a departure from the bonding in the "5-3-6" structure (above) and the "4-3-4" and "3-2-3" structures discussed in a previous publication [12]. Such high DOS at the Fermi level is not in agreement with the simple ways to rationalize the structure, following the octet rule and the Zintl concept. If one were to do so, the charge-balanced formula $[A^{2+}]_3[(4b\text{-}In^{1-})_2(3b\text{-}Ge^{1-})_4]$ would contradict the *ab-initio* calculations.

What could have happened? The answer of this question comes from interrogating the bonding in a hypothetical structure (Fig. 7(a)). DOS and COHP curves for it are projected in Fig. 7(b). Here, one immediately notices that moving the Ge2 atom away from the mirror plane provides an appreciable decrease of the TDOS at the Fermi level. More importantly, the antibonding character of the Ge bonds within the now corrugated chain also decreases significantly, becoming nearly non-bonding from ca. −1.5 to −0.2 eV. This is a strong proof that the planar Ge chains with the $(tttctc)_n$ topology are not energetically favorable, and that the pyramidalization at the Ge2 site restricts the $\pi^*$ dispersion along the chain for stabilization of the chemical bonding. Similar effect has also been discussed on the examples of SrInGe and EuInGe [7], where the 3-bonded Ge zig-zag chain shows the onset of stereochemically active lone pairs. This theoretically derived explanation can be supported by experimental data as well—the diminished $\pi$-bonding in the Ge chains of $(Sr_{1-x}Ca_x)_3In_2Ge_4$ can be compared to those in $\alpha$-$Ca_2LiGe_3$, $\alpha$-$Sr_2LiGe_3$ and $Eu_2LiGe_3$ [34], and it can be related to the elongation of the Ge–Ge bonds, which typically indicates a decrease in the bond-order.

Another important result from the calculations on this structure model with "non-planar" Ge chains can also help us understand the elongated ADP of Ge2 along the *b*-axis. Its elongated oval shape (Fig. 4) is suggestive of an out-of-plane disorder as in the model, but trial refinements done by splitting the Ge2 site were not conclusive [37]. Presumably, the actual

deviation from the mirror plane is less than what we had in the model, i.e., less than 0.4 Å, which is difficult to refine with a satisfactory statistical significance. However, we noticed that when Ge2 is displaced from its averaged position at $y=0$, this results in an elongation of the Ge2–Ge3/4 distances up to ca. 2.67 Å. Such distances between neighboring Ge atoms would indicate very weak bonds; however, they could also represent very reasonable Ge–In bonds. This piqued our attention and we took a closer look at the TDOS in Fig. 7b—a pseudogap just below the Fermi level can be seen. The corresponding COHP curve also shows a sudden increase of the antibonding character beyond this point. Therefore, we can speculate that this might be an indication of a small admixture of In on the pyramidal Ge2 site, which lowers the number of valence electrons to its optimal level (ca. 0.7 fewer electrons), corresponding to an overall formula $(Sr1_{-x}Ca_x)_3In_{2.3}Ge_{3.7}$. Such conjecture is not only based on the net bonding optimization as a result of shifting the Fermi level to the pseudogap, but can also be supported by bond distances arguments. We note here that the possibility of having partially occupied In atoms at the Ge2 site ($x=0.3981(1)$; $y=0$; and $z=0.2231(1)$) can be ruled out based on the next-neighbor distances – 2.594(2) Å and 2.622(2) Å – which are unrealistic for In–Ge bonding [30]. However, the fact that the electron density at this site was found to be smeared and slightly higher (ca. 15%) than a fully occupied Ge, combined with the interpretation of the chemical bonding as discussed above, may indicate that the structural parameters of $(Sr_{1-x}Ca_x)_3In_2Ge_4$ represent the "average" structure. The real (local) structure of the "3-2-4" phase could indeed be closer to what we considered in our hypothetical model. Currently, attempts to synthesize other compounds with similar Ge-bonding and studying their structures and properties are under way.

## 4. Conclusions

We have successfully synthesized and characterized two novel intermetallic phases of $A_5In_3Ge_6$ and $A_3In_2Ge_4$ ($A$=Ca, Sr, Eu, Yb). These two phases exist only in mixed-cation systems, underscoring the importance of the cations' atomic sizes and electronegativities for the realization of a given crystal structure. The anion sub-network of $A_5In_3Ge_6$ is based upon chains of [$InGe_4$] tetrahedra, $Ge_4$ tetramers isosteric with 1,3-*cis*-butadiene, and distorted square-planar [$InGe_4$] fragments. The structure of $A_3In_2Ge_4$ is a combination of infinite Ge chains with *cis*- and *trans*-bonds in a complex $(tttctc)_n$ pattern, [$InGe_4$] tetrahedra, and In zig-zag chains. Electronic band structure calculations for both phases confirm the strong involvement of the cations in the overall bonding. In the case of the $A_3In_2Ge_4$ phase, the calculations also suggested that the antibonding character of the Ge bonding in the anionic segment can be greatly diminished by a small positional disorder at the Ge2 site, thereby leading to a "puckering" of the 3-bonded planar fragment. The origins of this effect can be traced to a second-order Jahn-Teller distortion in $M_2X_4$-like species [42]. Since the tendency for such pyramidalization will be more pronounced in Sn than in Ge (due to the worse *s–p* mixing), one could expect that if isomorphous $A_3In_2Sn_4$ phases can be synthesized, the crystallographic evidence for it will be more definitive.

## Acknowledgments

Svilen Bobev acknowledges financial support from the National Science Foundation through a grant DMR-0743916 (CAREER).

## References

[1] P. Villars, L.D. Calvert (Eds.), Pearson's Handbook of Crystallographic Data for Intermetallic Compounds, 2nd Ed., American Society for Metals, Materials Park, OH, USA 1991, and the desktop edition 1997.
[2] P.H. Tobash, D. Lins, S. Bobev, A. Lima, M.F. Hundley, J.D. Thompson, J.L. Sarrao, Chem. Mater. 17 (2005) 5567.
[3] V.I. Zaremba, D. Kaczorowski, G.P. Nychyporuk, U.C. Rodewald, R. Pöttgen, Solid State Sci. 6 (2004) 1301;
[b] V.I. Zaremba, D. Johrendt, U.C. Rodewald, G.P. Nychyporuk, R. Pöttgen, Solid State Sci. 7 (2005) 998.
[4] [a] V.I. Zaremba, D. Kaczorowski, G.P. Nychyporuk, U.C. Rodewald, B. Heying, R. Pöttgen, Z. Anorg. Allg. Chem. 632 (2006) 975;
[b] A.M. Guloy, J.D. Corbett, Inorg. Chem. 35 (1996) 2616.
[5] G. Nychyporuk, V. Zaremba, Ya.M. Kalychak, J. Stepien-Damm, A. Pietraszko, J. Alloys Compd. 312 (2000) 154.
[6] J.-G. Mao, A.M. Guloy, J. Alloys Compd. 322 (2001) 135.
[7] J.-G. Mao, J. Goodey, A.M. Guloy, Inorg. Chem. 41 (2002) 931.
[8] A. Bentien, E. Nishibori, S. Paschen, B.B. Iversen, Phys. Rev. B: Condens. Matter 71 (2005) 144107.
[9] [a] H.-G. von Schnering, R. Kröner, W. Carrillo-Cabrera, K. Peters, R. Nesper, Z. Kristallogr.—New Cryst. Struct. 213 (1998) 665;
[b] S.-J. Kim, S.-Q. Hu, C. Uher, T. Hogan, B.-Q. Huang, J.D. Corbett, M.G. Kanatzidis, J. Solid State Chem. 153 (2000) 321.
[10] Z.-H. Xu, A.M. Guloy, J. Am. Chem. Soc. 119 (1997) 10541.
[11] J.-G. Mao, Z.-H. Xu, A.M. Guloy, Inorg. Chem. 40 (2001) 4472.
[12] T.-S. You, P.H. Tobash, S. Bobev, Inorg. Chem. 49 (2010) 1773.
[13] V. Zaremba, Y.u.B. Tyvanchuk, J. Stepien-Damm, Z. Kristallogr.—New Cryst. Struct. 212 (1997) 291.
[14] [a] E.I. Gladyshevskii, Dopov. Akad. Nauk 2 (1964) 209;
[b] S. Bobev, E.D. Bauer, J.D. Thompson, J.L. Sarrao, G.J. Miller, B. Eck, R. Dronskowski, J. Solid State Chem. 177 (2004) 3545.
[15] O. Schob, E. Parthe, Acta Crystallogr. 19 (1965) 214.
[16] P.H. Tobash, S. Bobev, J. Solid State Chem. 180 (2007) 1575.
[17] G. Bruzzone, Acta Crystallogr. 18 (1965) 1081.
[18] Bruker *SMART*, Bruker AXS Inc., Madison, Wisconsin, USA, 2002.
[19] Bruker *SAINT*, Bruker AXS Inc., Madison, Wisconsin, USA, 2002.
[20] G.M. Sheldrick, SADABS, University of Göttingen, Germany, 2003.
[21] G.M. Sheldrick, SHELXTL, University of Göttingen, Germany, 2001.
[22] L.M. Gelato, E. Parthe, J. Appl. Crystallogr. 20 (1987) 139.
[23] [a] O.K. Andersen, Phys. Rev. B 12 (1975) 3060;
[b] O.K. Andersen, O. Jepsen, Phys. Rev. Lett. 53 (1984) 2571;
[c] O.K. Andersen, Phys. Rev. B 34 (1986) 2439.
[24] O. Jepsen, A. Burkhardt, O.K. Andersen, The TB-LMTO-ASA Program, version 4.7; Max-Planck-Institut für Festkorperforschung: Stuttgart, Germany, 1999.
[25] O.K. Andersen, O. Jepsen, D. Glötzel, in: F. Bassani, F. Fumi, M. Tosi (Eds.), Highlights of Condensed Matter Theory, NewYork, North-Holland, Lam- brecht, W. R. L., 1985.
[26] O. Jepsen, O.K. Anderson, Z. Phys. B 97 (1995) 35.
[27] O.K. Anderson, O. Jepsen, Phys. Rev. Lett. 53 (1984) 2571.
[28] R. Dronskowski, P. Blöchl, J. Phys. Chem. 97 (1993) 8617.
[29] P.E. Blöchl, O. Jepsen, O.K. Anderson, Phys. Rev. B 49 (1994) 16223.
[30] L. Pauling, The Nature of the Chemical Bond, Cornell University Press, Ithaca, NY, 1960.
[31] A.-V. Mudring, J.D. Corbett, J. Am. Chem. Soc. 126 (2004) 5277.
[32] A. Palenzona, M. Pani, J. Alloys Compd. 402 (2005) 136.
[33] R.D. Shannon, Acta Crystallogr. Sect. A 32 (1976) 751.
[34] [a] W. Müller, H. Schäfer, A. Weiss, Z. Naturforsch. B: Chem. Sci. 26 (1971) 5;
[b] Q.-X. Xie, R. Nesper, in: Proceedings of the Ninth European Conference on Solid State Chemistry, P106, Stuttgart, Germany, 2003;
[c] Q.-X. Xie, R. Nesper, Z. Kristallogr.—New Cryst. Struct. 219 (2004) 79.
[35] B. Li, S.-J. Kim, G.J. Miller, J.D. Corbett, Inorg. Chem. 48 (2009) 6573.
[36] B. Li, J.D. Corbett, Inorg. Chem. 45 (2006) 2960.
[37] Refinements in lower symmetry groups, such as *C*2, were unsuccessful. Despite the increased number of variables, the fits were generally poorer. In particular, the *y* coordinate of the Ge2 site did not deviate significantly from zero ($y=0.0014(3)$), and the electron density at this position remained rather "smeared".
[38] [a] S. Bobev, S.C. Sevov, J. Am. Chem. Soc. 121 (1999) 3795;
[b] S. Bobev, S.C. Sevov, J. Solid State Chem. 153 (2000) 92;
[c] S. Bobev, S.C. Sevov, Inorg. Chem. 39 (2000) 5930.
[39] J.H. Westbrook, R.L. Fleisher (Eds.), Intermetallic Compounds: Principle and Practices, Wiley, New York, 1995.
[40] [a] H. Schäfer, Annu. Rev. Mater. Sci. 5 (1985) 1;
[b] R. Nesper, Prog. Solid State Chem. 20 (1990) 1;
[c] S.M. Kauzlarich (Ed.), Chemistry, Structure and Bonding in Zintl Phases and Ions, VCH, New York, 1996 and the references therein.
[41] [a] S.-Q. Xia, S. Bobev, Inorg. Chem. 47 (2008) 1919;
[b] S.-Q. Xia, S. Bobev, J. Am. Chem. Soc. 129 (2007) 4049;
[c] S.-Q. Xia, S. Bobev, J. Am. Chem. Soc. 129 (2007) 10011.
[42] T.A. Albright, J.K. Burdett, M.-H. Whangbo, Orbital Interactions in Chemistry, Wiley-Interscience, New York, 1985.